Brain Topogr (2015) 28:5–20
DOI 10.1007/s10548-014-0417-z

ORIGINAL PAPER

Catching the Invisible: Mesial Temporal Source Contribution to Simultaneous EEG and SEEG Recordings

Laurent Koessler · Thierry Cecchin · Sophie Colnat-Coulbois · Jean-Pierre Vignal · Jacques Jonas · Hervé Vespignani · Georgia Ramantani · Louis Georges Maillard

Received: 14 May 2014 / Accepted: 8 November 2014 / Published online: 29 November 2014
© Springer Science+Business Media New York 2014

Abstract Mesial temporal sources are presumed to escape detection in scalp electroencephalographic recordings. This is attributed to the deep localization and infolded geometry of mesial temporal structures that leads to a cancellation of electrical potentials, and to the blurring effect of the superimposed neocortical background activity. In this study, we analyzed simultaneous scalp and intracerebral electroencephalographic recordings to delineate the contribution of mesial temporal sources to scalp electroencephalogram. Interictal intracerebral spike networks were classified in three distinct categories: solely mesial, mesial as well as neocortical, and solely neocortical. The highest and earliest intracerebral spikes generated by the leader source of each network were marked and the corresponding simultaneous intracerebral and scalp electroencephalograms were averaged and then characterized both in terms of amplitude and spatial distribution. In seven drug-resistant epileptic patients, 21 interictal intracerebral networks were identified: nine mesial, five mesial plus neocortical and seven neocortical. Averaged scalp spikes arising respectively from mesial, mesial plus neocortical and neocortical networks had a 7.1 ($n = 1{,}949$), 36.1 ($n = 628$) and 10 ($n = 1{,}471$) μV average amplitude. Their scalp electroencephalogram electrical field presented a negativity in the ipsilateral anterior and basal temporal electrodes in all networks and a significant positivity in the fronto-centro-parietal electrodes solely in the mesial plus neocortical and neocortical networks. Topographic consistency test proved the consistency of these different scalp electroencephalogram maps and hierarchical clustering clearly differentiated them. In our study, we have thus shown for the first time that mesial temporal sources (1) cannot be spontaneously visible (mean signal-to-noise ratio −2.1 dB) on the scalp at the single trial level and (2) contribute to scalp electroencephalogram despite their curved geometry and deep localization.

Keywords Simultaneous EEG–SEEG recordings · Deep brain sources · Source localization · Mesial temporal lobe epilepsy · Hippocampus · Volume conduction

Abbreviations

IIS	Interictal intracerebral spikes
ISS	Interictal scalp spikes
M	Mesial epileptic network
NC	Neocortical epileptic network
M + NC	Mesial and neocortical epileptic network
MTL	Mesial temporal lobe
SEEG	Stereoelectroencephalography

Electronic supplementary material The online version of this article (doi:10.1007/s10548-014-0417-z) contains supplementary material, which is available to authorized users.

L. Koessler (✉) · T. Cecchin · J.-P. Vignal · J. Jonas · H. Vespignani · G. Ramantani · L. G. Maillard
UMR 7039, CRAN, CNRS - Université de Lorraine, 2 Avenue de la forêt de Haye, 54516 Vandoeuvre-Lès-Nancy, France
e-mail: laurent.koessler@univ-lorraine.fr

L. Koessler · T. Cecchin · J.-P. Vignal · J. Jonas · H. Vespignani · G. Ramantani · L. G. Maillard
UMR 7039, CRAN, CNRS, Vandoeuvre-Lès-Nancy, France

L. Koessler · J.-P. Vignal · J. Jonas · H. Vespignani · L. G. Maillard
Service de Neurologie, Centre Hospitalier Universitaire de Nancy, 54000 Nancy, France

S. Colnat-Coulbois
Service de Neurochirurgie, Centre Hospitalier Universitaire de Nancy, Nancy 54000, France

G. Ramantani
Epilepsy Center, University Hospital Freiburg, 79106 Freiburg, Germany

Introduction

The contribution of electrical potentials arising from deep brain sources in scalp EEG recordings is still under debate. This issue is particularly crucial in temporal lobe epilepsy, due to the involvement of complex mesial and/or neocortical, epileptogenic networks (Maillard et al. 2004; Barba et al. 2007; Bartolomei et al. 2008). Currently, it is widely accepted that localized hippocampal interictal or ictal discharges do not correspond to concomitant visible correlates in scalp EEG (International League against Epilepsy commission's report of the electroclinical features of mesial temporal lobe (MTL) epilepsy; Wieser 2004). Thus, evidence of MTL involvement in refractory partial epilepsy is commonly indirect, deriving from seizure semiology and hippocampal sclerosis in structural- and/or hypometabolism in functional imaging (Gil-Nagel and Risinger 1997; Williamson et al. 1998; Chassoux et al. 2004). The indication for MTL resection is set when the sum of criteria is fulfilled. Otherwise, direct evidence of MTL involvement in the epileptogenic network derives solely from intracerebral recordings with depth electrodes. The identification of scalp EEG biomarkers of MTL involvement is therefore crucial for the delineation and differentiation of mesial from neocortical sources, since this may constitute a potential surrogate for invasive recordings (Harroud et al. 2012).

This issue has been previously addressed by comparative studies of simultaneous intracranial and scalp EEG recordings that facilitate the study of cortical potential contribution to scalp EEG recordings. These studies derive from invasive investigations performed mainly with foramen ovale or subdural electrodes (Baumgartner et al. 1995; Alarcon et al. 1994, 1997; Lantz et al. 1996; Merlet et al. 1998; Nayak et al. 2004; Yamazaki et al. 2012; Wennberg and Cheyne 2014) and seldom with depth electrodes (Abraham and Ajmone-Marsan 1958; Lieb et al. 1976; Alarcon et al. 1994). These studies, deriving from the routine visual analysis of concomitant scalp EEG, have supported that interictal (Alarcon et al. 1994; Merlet et al. 1998) or ictal discharges (Lieb et al. 1976) confined to MTL structures escape detection in scalp EEG recordings. This was primarily attributed to physical reasons, including (1) the specific geometric and anatomic configuration of MTL structures (Sedat and Duvernoy 1990) that produce a presumably closed electrical field (Jayakar et al. 1991; Ebersole 2000), (2) the distance between MTL structures and scalp electrodes (Lopes Da Silva and Van Rotterdam 1993), and (3) the amplitude of background activity originating from basal and lateral neocortical regions that towers over the conducted MTL signals (Mikuni et al. 1997). Further studies, deriving from the analysis of averaged scalp EEG concomitant with intracranial signals, have suggested that temporal lobe sources are detectable in scalp EEG only if interictal or ictal discharges (1) are not solely confined to MTL structures and (2) simultaneously involve the lateral part of the temporal lobe (Alarcon et al. 1994; Lantz et al. 1996; Merlet and Gotman 1999; Wennberg and Cheyne 2014). However, the major limitation of these observations relying on foramen ovale or subdural electrodes is the inherent difficulty to disentangle the activity generated by solely mesial from the activity generated by neocortical sources with electrodes placed in the vicinity of—as opposed to within the MTL. Thus, there is an urgent need to address the question of purely MTL contribution to scalp EEG potentials deriving from intracerebral hippocampal, subhippocampal and neocortical recordings.

In this study, epileptic sources localized solely in mesial (M), in mesial as well as neocortical (M + NC) and solely in neocortical (NC) temporal regions, as defined by stereoelectroencephalography (SEEG) recordings, were investigated with simultaneous scalp and intracerebral EEG recordings to comparatively assess the contribution of MTL and neocortical sources to scalp EEG signals.

Materials and Methods

Patients

Seven patients (three female) with temporal lobe epilepsy (TLE, three right TLE) and a mean age of 38 years (Table 1) were selected from 40 consecutive patients that underwent simultaneous scalp EEG and SEEG recordings in the context of presurgical investigations for refractory partial epilepsy in 2009–2012 in the University Hospital of Nancy, France. Prior comprehensive evaluation included a detailed medical history, full neurological examination, neuropsychological assessment, high resolution MRI, interictal PET, interictal and ictal (when available) SPECT, and 64-channel long-term scalp video-EEG recordings, as well as electrical source imaging (Maillard et al. 2009; Koessler et al. 2010). We enrolled patients with (1) an epileptogenic zone confined to the temporal lobe and (2) at least one interictal intracerebral spike (IIS) source confined to the MTL, as defined by SEEG recordings. All patients gave their informed consent prior to participation. The study was granted approval by the local ethics committee.

Intracerebral and Scalp EEG Electrodes

SEEG was performed using 0.8 mm-diameter depth electrodes with 8–15 2 mm-long contacts per electrode and a 1.5 mm intercontact distance (DIXI Microtechniques, Besançon, France). For electrode placement, a Leksell G-frame (Elekta, Stockholm, Sweden) was positioned on

Table 1 Main clinical features of all seven patients (P1–P7)

Patients	Gender	Age (years)	Epileptogenic zone defined by SEEG	Laterality	MRI	Interictal EEG	Surface electrodes	Depth electrodes
P1	M	49	Mesial	R	bilateral HS	R temporal slow waves—spikes	8	9 (R) + 3 (L)
P2	F	27	Mesial, pole	R	DNT	R temporal slow waves—no spikes	25	8 (R) + 1 (L)
P3	M	32	Mesial	L	Normal	L ant. temporal spikes	14	2 (R) + 9 (L)
P4	M	51	Mesial	L	L HS	L ant. temporal slow waves—spikes	14	1 (R) + 10 (L)
P5	F	46	Mesial, pole	L	L HS	L ant. temporal spikes	14	1 (R) + 8 (L)
P6	M	29	Mesial, ant. and mid. basal part	L	L ITG atrophy	L mid. temporal slow waves—spikes	13	1 (R) + 8 (L)
P7	F	31	Mesial, pole, insula	R	R HS and pole atrophy	R mid. temporal slow waves—spikes	21	10 (R) + 2 (L)

IIS interictal intracerebral spikes, *M* mesial, *NC* neocortical, *F* female, *M* male, *y* years, *L* left, *R* right, *ant* anterior, *mid* middle, *HS* hippocampal sclerosis, *DNT* dysembryoplastic neuroepithelial tumor, *ITG* inferior temporal gyrus

the patient's head and a stereotactic MRI (3D SPGR T1-weighted sequence with double injection of gadolinium) was performed. The MRI was subsequently imported into a computer-assisted stereotactic module (Leksell Surgiplan®; Elekta, Stockholm, Sweden) and electrode trajectories were delineated according to the presurgical implantation scheme, carefully avoiding vascular structures. The presurgical implantation scheme derived from a standardized approach simultaneously sampling mesial, basal and lateral temporal lobe structures that was individually adapted according to the presumed localization of the epileptogenic and propagation zones (Koessler et al. 2010; Ramantani et al. 2013). A postoperative stereotactic CT was performed and fused with the preoperative MRI to determine the exact position of each intracerebral contact. These positions have been carefully checked by the investigators (SCC, LGM and JPV).

The following structures were sampled in all patients: amygdala; anterior and posterior hippocampus; entorhinal cortex; collateral fissure; parahippocampal gyrus; internal and external temporal pole; superior, middle and inferior temporal gyri; temporo-occipital junction; fusiform gyrus; insula.

In average, 10 ± 2 depth electrodes were placed within the temporal lobe ipsilateral to the presumed epileptogenic zone and 1.5 ± 1 depth electrodes were placed in the contralateral temporal lobe, amounting to an average of 90 intracerebral contacts in total. The scalp EEG was mounted using 16 ± 6 sterile Ag/AgCl electrodes of 10 mm diameter (Table 1). Occasionally one or two scalp electrodes were slightly displaced from the standard positions of the 10–20 system, due to the surgical scars resulting from depth electrode insertion. Scalp electrode positions were calculated by a 3D digitizer system (3 Space Fastrak; Polhemus, Colchester, VT, USA). Two main scalp regions were sampled: the fronto-centro-parietal region and the lateral and basal temporal regions ipsi- and contralateral to the presumed epileptogenic zone (F9/F10, FT9/FT10, P9/P10, AF7/AF8, T7/T8; Koessler et al. 2009). Further electrodes were occasionally placed (F7/F8, Fp1/Fp2, P7/P8, C5, FC5, CP5, O1/O2, Oz) according to the spatial distribution of interictal spikes in 64-channel EEG recordings and the respective electroclinical hypothesis.

Simultaneous EEG and SEEG Recordings

Simultaneous EEG and SEEG recordings were performed using a 128 channel system (LTM128; Micromed, Beaune, France). The EEG and SEEG acquisition signals were referenced to the Fpz scalp electrode. Signals were sampled at 512 Hz and filtered with an analog 0.15 Hz high-pass filter. Simultaneous EEG and SEEG recordings were performed for 5 days, 20/24 h. 2–3 h of simultaneous scalp EEG and SEEG recordings during calm wakefulness were selected for interictal spike analysis, avoiding ictal events or preictal changes.

Data Collection and Analysis

Data collection and analysis were performed in four consecutive steps: (1) interictal intracerebral spike (IIS) selection and characterization, (2) IIS network classification, (3) averaged interictal scalp spike (ISS) validation and characterization and (4) averaged ISS automatic clustering (Fig. 1).

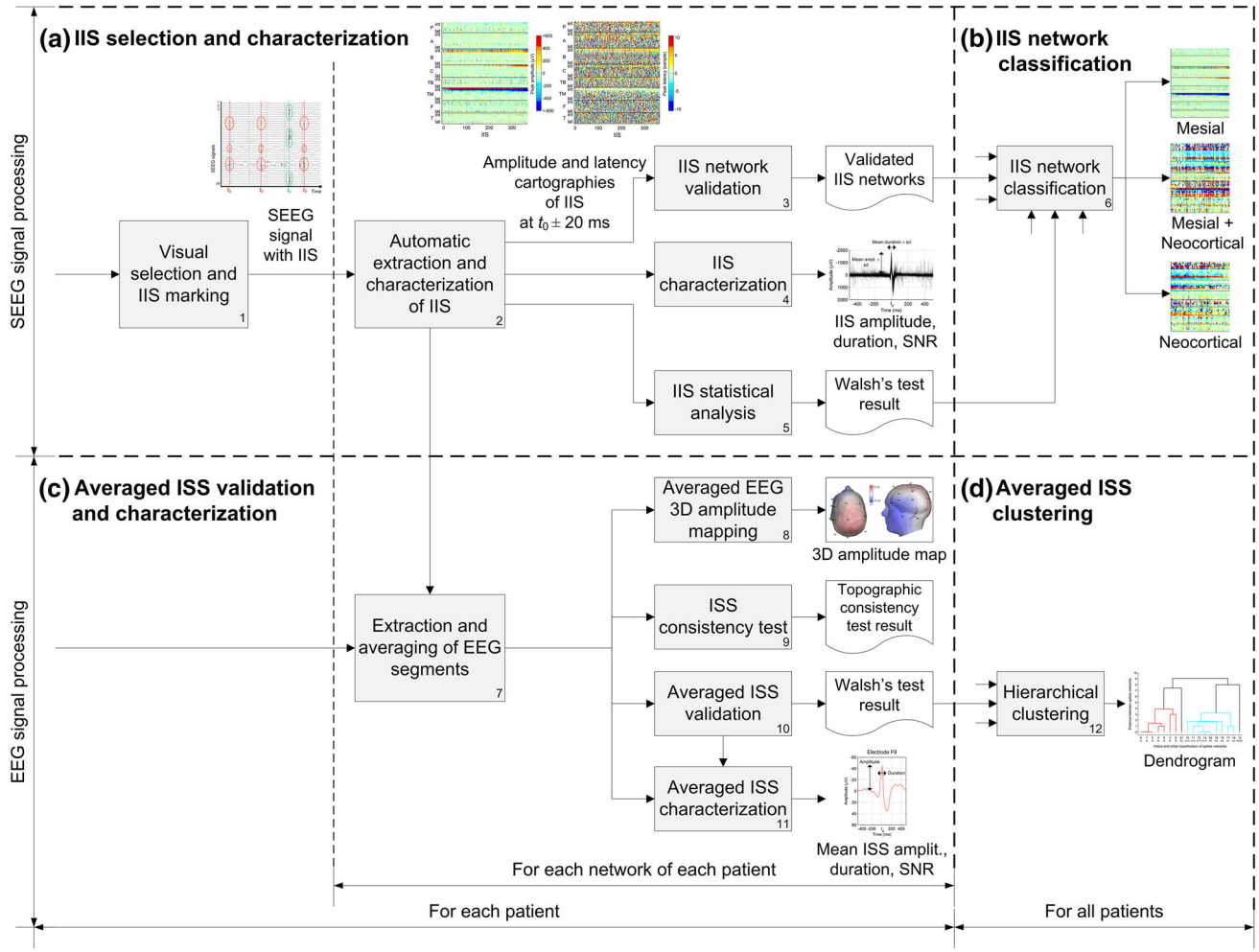

Fig. 1 Overview of data collection and analysis. *IIS* interictal intracerebral spikes, *ISS* interictal scalp spikes, *SNR* signal-to-noise ratio

Interictal Intracerebral Spike (IIS) Selection and Characterization

IIS Visual Selection and Classification

SEEG recordings were visually analyzed by three experienced neurophysiologists (LK, LGM and JPV) using a bipolar montage, that provides the potential difference between two contiguous contacts and discards events generated by far field potentials, thus exclusively depicting events from focal and adjacent sources. The IIS were identified according to the definition of the International Federation of the Society for Electroencephalography and Clinical Neurophysiology (IFSECN) as transient events, clearly distinguishable from the background activity (at least two times higher in amplitude), with a pointed peak at conventional screen display and a duration from 20 to less than 70 ms (Chang et al. 2011a). The main component of these IIS was generally negative and had variable amplitude. For each patient, IIS networks were defined by the reproducible co-occurrence of IIS in different temporal lobe structures. These IIS networks were classified as: mesial (M) if IIS co-occurred within the MTL comprising the amygdala, hippocampus, entorhinal cortex, parahippocampal gyrus and collateral sulcus; neocortical (NC) if IIS co-occurred within any other temporal neocortical structures lateral to the collateral sulcus (fusiform, inferior, middle, and superior temporal gyri) and mesial plus neocortical (M + NC) if IIS co-occurred within both MTL and neocortical structures. This classification has been previously validated for ictal discharges on both clinical and neurophysiological grounds (Bartolomei et al. 2001; Maillard et al. 2004). Within each of these networks, the earliest IIS with the highest amplitude were manually marked with a trigger (t_0) at the peak of the initial component for subsequent averaging; the corresponding source was considered the leader source of the network.

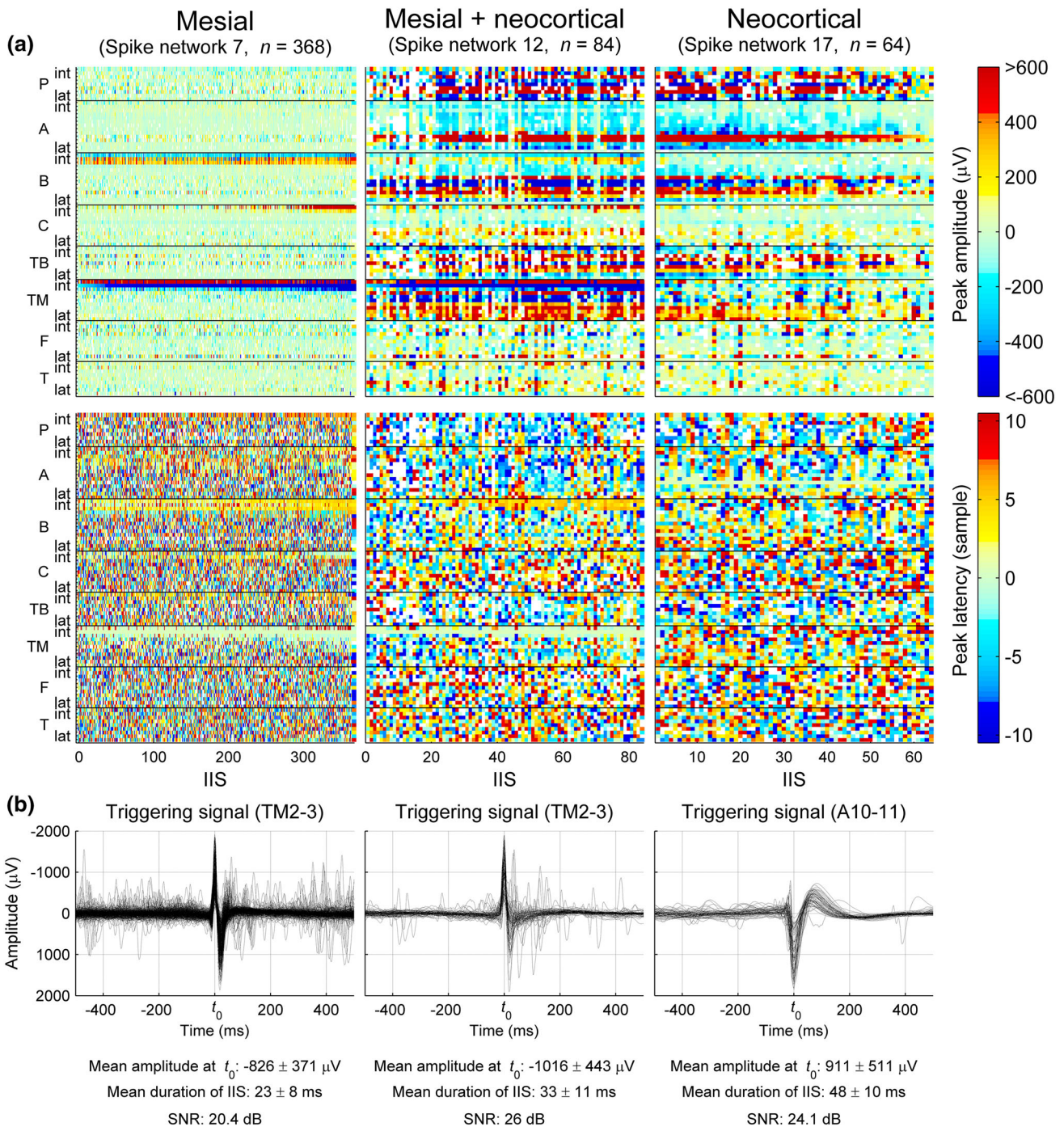

Fig. 2 SEEG characterization for the three distinct IIS networks in patient 5. **a** Spatial and temporal distributions of the three networks depicted by condensed amplitude and latency cartographies around $t_0 \pm 20$ ms. The *IIS* are sorted by increasing peak amplitude values: e.g. in the M network the highest spike amplitudes were observed in the internal contacts of *TM*, *B* and *C* (located in hippocampus) with a phase reversal in *TM* and *B*. The earliest spikes were observed in the internal contacts of *TM* and followed by spikes in the internal contacts of B with a 5 ms delay. **b** Overlay of each segment recorded in the same contact of the highest and earliest peak and their characteristics at t_0

IIS Automatic Extraction, Characterization and IIS Network Validation

Condensed cartographies of IIS amplitude and latency (Fig. 2a) were obtained for each network in order to (1) ascertain that the selected IIS was indeed the earliest event with the highest amplitude within the network, and to (2) verify that all individual spikes presented an identical intracerebral distribution and therefore belonged to the same network.

For this purpose, SEEG segments of 1 s centered on t_0 were automatically extracted. For each SEEG segment, local extremes corresponding to IIS were automatically detected within an interval of ±10 samples (±19.5 ms) around the trigger instant (t_0). The amplitude and latency of this extreme were automatically calculated. All values of amplitude and latency at t_0 were converted into a corresponding color scale (Fig. 2a). SEEG segments without a peak were coded with white.

IIS Characterization

For each IIS, we computed the amplitude, duration and signal-to-noise ratio (SNR) at t_0 in the triggering channel (Fig. 2b). SEEG signals were filtered with a 1.5 Hz high-pass filter that allowed suppressing slow baseline drifts. Spike duration was generally estimated automatically as the latency between the first detected time-axis crossing before and after t_0. In case of baseline fluctuation that would lead to an overestimation of spike duration by this approach, we commenced the analysis from the spike peak at t_0 and searched for the extremes around the peak. For SNR computation of the whole set of IIS, we proceeded as follows. Let $x(i,t)$ be the value of the filtered triggering signal of the ith recording ($i = 1,\ldots, n$) at time t, we had:

$$x(i, t_0) = s(i) + v(i, t_0)$$

where $s(i)$ represents the peak value of the spike for the ith recording and $v(i,t)$ the "noise", that is the background activity. We assumed that $s(i)$ and $v(i,t)$ were random variables and that v had a zero mean. We defined the SNR as:

$$\mathrm{SNR(dB)} = 10\log_{10}\left(\frac{\mathrm{E}[s^2]}{\sigma_v^2}\right)$$

Here E[.] denotes the expected value and σ_v^2 the variance of v. To estimate this variance, we first extracted the values corresponding to $[-500,-250] \cup [250,500]$ ms for each IIS segment; we assumed that these intervals contained only noise and that the spike was contained in the interval $[-250,250]$ ms. We further concatenated all intervals corresponding to the n IIS in a single vector representing the variance.

IIS Statistical Analysis of M Networks

For M network, in order to check that non-mesial contacts were not activated at time zero during the discharges classified as purely mesial, we performed a *quantitative* validation. Each IIS were compared to background activity, in every intracerebral contact, by a statistical test of outlier rejection under the null hypothesis that the amplitude of the peak did not significantly differ from the amplitude of the background activity as measured in the intervals $[-500, -250]$ and $[250,500]$ ms around t_0. We used the Walsh nonparametric test (Walsh 1959), since preliminary tests indicated that the background activity was not normally distributed. The significance level was set at $\alpha = 0.05$. Then, we computed the percentage of significant response (positivity or negativity) in non-mesial contacts.

IIS Network Classification

Condensed cartographies with similar IIS distribution were concatenated and classified using visual expert and statistical analysis (see "IIS statistical analysis" section) into one of three distinct categories (Fig. 2a): (1) M if IIS were recorded only within mesial temporal structures (i.e. anterior and posterior hippocampus, entorhinal cortex, parahippocampal and collateral fissure); (2) NC if IIS were recorded in structures lateral to the collateral fissure (i.e. basal and lateral part of the temporal lobe); (3) M + NC if IIS were recorded simultaneously or within a maximum latency of 20 ms in both mesial and neocortical temporal structures.

Averaged Interictal Scalp Spike (ISS) Validation and Characterization

Extraction and Averaging of Scalp EEG Segments

Scalp EEG segments were extracted using the same 1 s epoch centered on t_0 as SEEG segments. Segments with scalp EEG amplitude >150 μV that represented <10 % of all segments were rejected as artifacts. The remaining segments were band-pass filtered with cut-offs at 1.5 and 30 Hz and averaged using the same t_0 triggers as for simultaneous IIS (Fig. 3).

Visual Analysis of Averaged EEG 3D Amplitude Maps

Realistic head models (boundary element models: BEM) and 3D amplitude cartographies were used to delineate the propagation of cortical sources to the scalp. The head models were obtained from the individual MRI by a semi-automatic segmentation procedure (ASA software, Enschede, The Netherlands). The 3D positions of scalp electrodes in each patient were digitized and subsequently co-registered with the 3D head reconstruction using fiducial landmarks (nasion, left and right tragus). 3D amplitude maps served to represent the amplitude distribution of the averaged EEG segments at t_0 (Fig. 4b; supplementary figures). The amplitude values between electrodes were interpolated by 3D spline functions. In order to compare the scalp projections of all IIS networks, regardless of their lateralization, all corresponding averaged ISS were

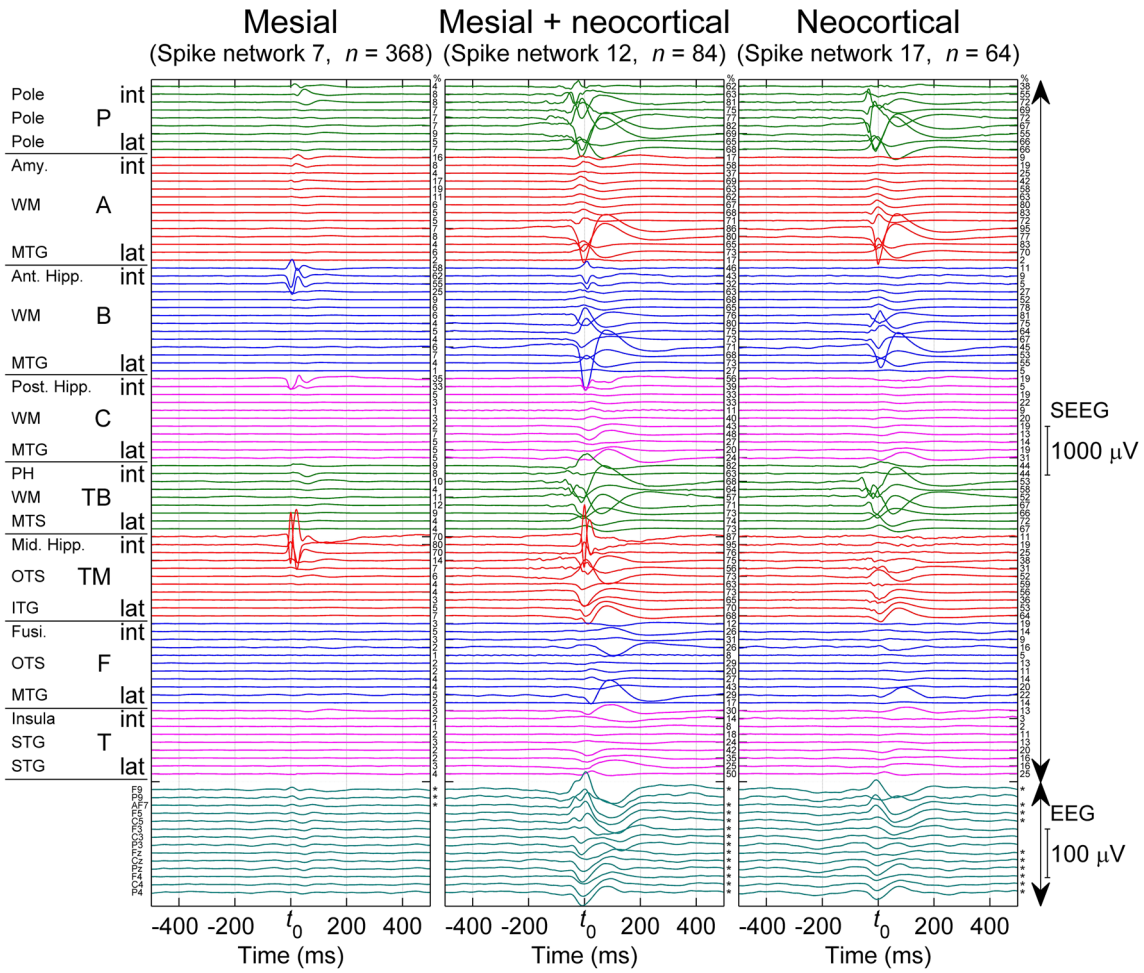

Fig. 3 Averaged simultaneous SEEG and EEG spikes corresponding to the three different spike networks in patient 5 and the percentage of significant responses (negative or positive; Walsh's test) at t_0, compared to the background activity, for each intracerebral derivation using un-averaged signals. The stars on the right of averaged EEG signals indicate that these signals were statistically significant (Walsh's test) at t_0. The spike networks 7, 12 and 17 were classified into: M network (anterior and mid hippocampus: B_{int} and TM_{int}); M + NC network (hippocampus: B_{int}, TM_{int}; PH: TB_{int}, temporal pole: $P_{int/lat}$, anterior MTG: A_{lat}, ITG and Fusiform gyrus: B_{mid}, TB_{mid}, TM_{mid}); and NC network (temporal pole: P_{lat}; MTG: A_{lat}; ITG and fusiform gyrus: B_{mid}, TB_{mid}, TM_{mid}). *Amy*. Amygdala, *WM* white matter, *MTG* middle temporal gyrus, *Ant. Hipp* anterior hippocampus, *Post. Hipp* posterior hippocampus, *PH* para-hippocampal cortex, *MTS* middle temporal sulcus, *Mid. Hipp* middle hippocampus, *OTS* occipito-temporal sulcus, *ITG* inferior temporal gyrus, *Fusi.* fusiform gyrus, *OTS* occipito-temporal sulcus, *STG* superior temporal gyrus; t_0: trigger instant)

represented with the highest negativity in the left hemispheric scalp electrodes.

Statistical Analysis of Averaged EEG and Validation of ISSs

For each network, we performed a *qualitative* assessment of averaged ISS as to the morphology, amplitude and duration of the visually detected peak and the background activity. Furthermore, we also performed a *quantitative* validation of averaged ISS compared to background activity in every scalp electrode by the same statistical test used for IIS i.e. a test of outlier rejection under the null hypothesis that the averaged amplitude of the peak did not significantly ($\alpha = 0.05$) differ from the averaged amplitude of the background activity. Combination of qualitative and quantitative assessments was used to determine if averaged EEG signals corresponded to epileptic spikes or not.

Averaged ISS Characterization

For each validated averaged ISS, we calculated the amplitude and duration in the scalp electrode with the highest negativity using the same method as for IIS (Fig. 4a; supplementary figures). For SNR determination of averaged ISS, we proceeded as follows:

Let $y(t)$ be the value of the considered averaged ISS segment at time t, we had:

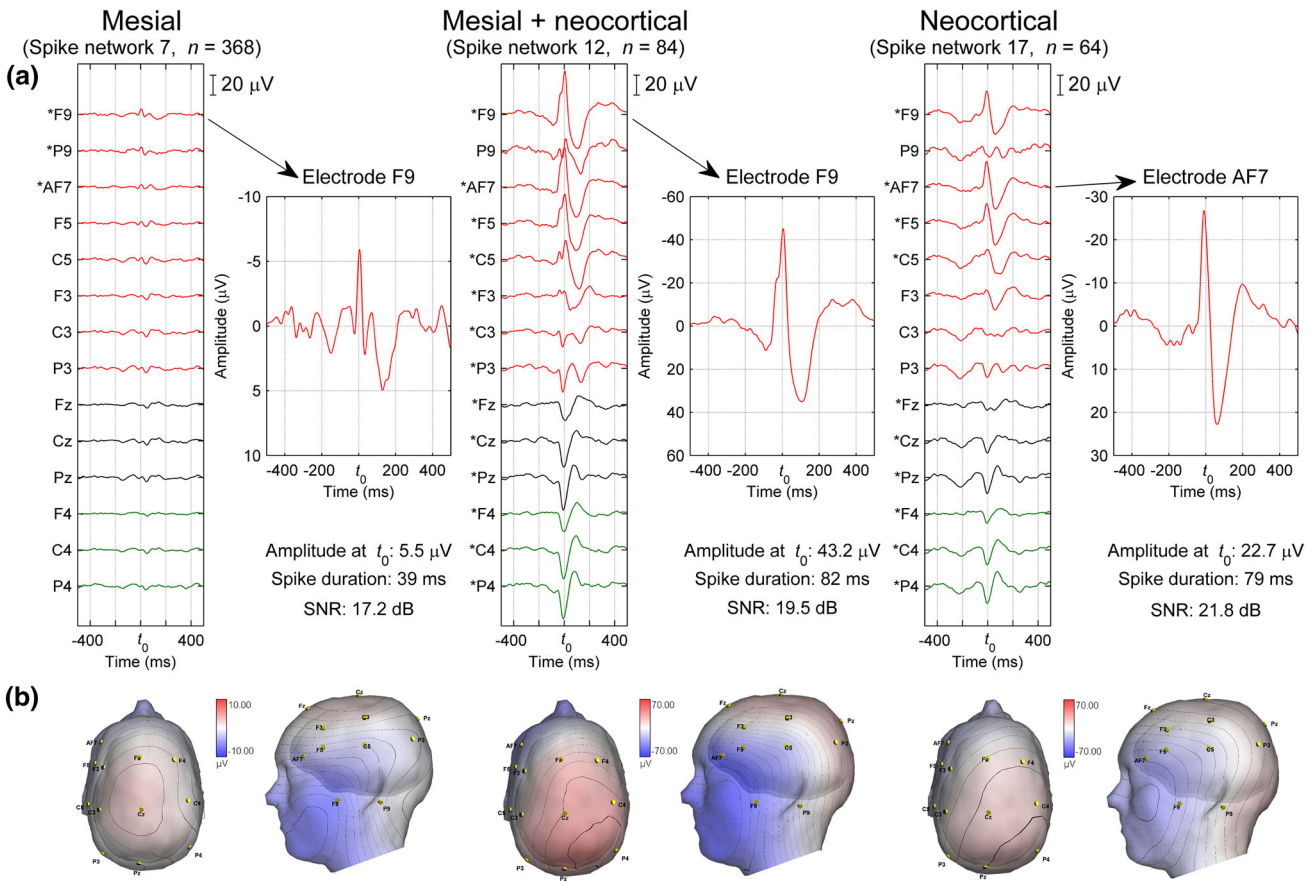

Fig. 4 **a** Averaged EEG signal and interictal scalp spike (ISS) characterization. The *stars* on the *left* of the electrode labels indicate that the corresponding averaged EEG signals at t_0 were statistically significant (Walsh's test) and thus validated as ISS. **b** 3D amplitude maps for the three distinct spike networks in patient 5. Additional figures for the other patients are given in supplementary figures

$$y(t_0) = u + w(t_0)$$

where u represents the spike value at t_0 and $w(t)$ the background activity. We assumed that $w(t)$ was a random variable with a zero mean and a variance equal to σ_w^2. Then, we defined the SNR as:

$$\mathrm{SNR(dB)} = 10\log_{10}\left(\frac{u^2}{\sigma_w^2}\right)$$

The estimation of σ_w^2 was made using the averaged ISS segment values corresponding to $[-500,-250] \cup [250,500]$ ms.

In addition, the SNR of un-averaged EEG signals were computed in the same way as for the averaged EEG signals to obtain the mean SNR of each network.

Topographic Consistency Test

In order to look for ISS distribution consistency, we used the topographic consistency test (Koenig and Melie-García 2010) on all networks. We computed the Global Field Power, time-instant by time-instant, within a time window corresponding to [−500, 500] ms around t_0 with a number of observations varying between 48 and 668, a number of sensors varying between 8 and 25, depending of the considered network, and with 500 randomization runs. A false discovery rate (FDR) criterion of 5 % was applied.

Averaged ISS Clustering

We applied hierarchical clustering to verify in an automatic way (i.e. independent from expert visual analysis) the classification of averaged ISS distributions obtained by visual analysis (Van 't Ent et al. 2003). The automatic and expert classifications were expected to match if IIS networks (1) were physiologically relevant, and (2) corresponded to distinct and reproducible averaged scalp electrical fields.

To overcome the issue of inter- and intra-subject spike variability, we considered only the presence or absence of a spike on averaged EEG signals. Walsh's test results were used as an indicator of spike presence. Thus, the input data for hierarchical clustering was a matrix **H** of r rows (the network number for all patients) and e columns (the total

number of different electrodes for all patients). In each cell of the matrix, the presence or absence of spike was coded as following: "+1″ for the spike positivity; "−1" for the spike negativity; "0" for the absence of a significant spike. The partially irregular positioning of EEG electrodes resulted in missing values, especially among those contralateral to the presumed epileptogenic zone. In order to reduce the ratio of missing values, we normalized the lateralization of epileptic foci: the left side was chosen as a reference and all right-sided foci were permuted to the left. The data of patient 1 (M networks 1 and 2) were not included in the analysis due to the limited scalp electrode coverage ($n = 8$) and the missing values in the data matrix. Consequently, the matrix was built with 18 IIS networks (rows) and 11 groups of EEG electrodes (columns).

Hierarchical clustering aimed at sorting spike networks into groups so that the degree of association between two networks would be maximal if they belonged to the same group and minimal otherwise. The first step consisted in estimating the similarity or dissimilarity between every pair of rows in the data matrix, quantified as a distance variable. We selected the *city-block* distance that is especially relevant for discrete data sets. Spike networks were further grouped into a hierarchical tree, i.e. dendrogram. We chose the unweighted average distance as a linkage function: the lower the distance, the higher the similarity between two ISS distributions. The final ISS distributions were classified according to the visual analysis of the dendrogram.

Results

Interictal Intracerebral Spike (IIS) Characterization

A total of 4,048 IIS were selected in all seven patients, corresponding to 578 IIS/patient or 193 IIS/network. Twenty-one IIS networks were validated and classified into (1) nine M networks encompassing 1,949 IIS, (2) five M + NC networks with 628 IIS, and (3) seven NC networks with 1,471 IIS (Table 2). All nine M networks comprised sources localized in the anterior hippocampus, six included sources localized in the middle and/or posterior hippocampus, seven in the amygdala, and five in the para-hippocampal gyrus. Interestingly, mesial temporal epileptic sources were not fully synchronous, presenting a 2–10 ms latency between the maximum amplitudes of co-occuring mesial temporal spikes (Fig. 2). In non-mesial contacts, only 6.7 % had amplitudes at t_0 that significantly differ from the amplitude of the background activity using Walsh's test. Mean amplitude in non-mesial contacts was about 7.4 μV. These significant responses were visually inspected by three experienced neurophysiologists (LK, LGM and JPV) and none of them were considered as epileptic spikes (Patient 5, Fig. 3).

NC networks comprised five sources localized in the temporal pole, three sources localized in the middle temporal gyrus, nine basal temporal sources, including eight in the fusiform and one in the inferior temporal gyrus, and one in the superior temporal gyrus. All five M + NC networks comprised sources localized in the anterior hippocampus, the temporo-polar and basal temporal regions, three included sources localized in the para-hippocampal regions, and three additional MTL sources.

Across all 21 networks, IIS serving as triggers presented a mean amplitude at t_0 of 895 ± 310 μV and a duration of 44 ± 10 ms. Their mean SNR was 18.2 dB, ranging from 11.6 to 26 dB. For each type of network, IIS amplitude and duration were: M 729 ± 279 μV and 38 ± 11 ms; M + NC 1,236 ± 414 μV and 43 ± 10 ms; NC 969 ± 306 μV and 54 ± 9 ms (Figs. 2, 3, patient 5).

Visual Analysis of Averaged EEG 3D Amplitude Maps

The visual analysis of the averaged ISS 3D amplitude maps revealed two distinct patterns.

The first pattern was characterized by a low amplitude negativity in the ipsilateral anterior basal temporal electrodes (F9–FT9 or F10–FT10) and a low amplitude positivity in the midline electrodes (Cz). Amplitude interpolation localized the maximum negativity in a more anterior and inferior position corresponding to the cheekbone. This pattern was specific for M networks (Fig. 4b; supplementary figures).

The second pattern was characterized by a higher amplitude with a more widespread negativity in the left temporal electrodes. The highest negativity was recorded in the ispilateral anterior basal temporal electrodes (F9-FT9 or F10-FT10). This pattern was additionally characterized by a widespread positivity in the vertex with a contralateral fronto-centro-parietal predominance (F4, C4, P4). This pattern corresponded to the M + NC and to the NC networks (Fig. 4b; supplementary figures).

Only a single amplitude map, corresponding to a NC network (n 21), was discordant with the typical pattern of its category. This 3D amplitude map comprised a focal negativity in the fronto-central midline (Fz and Cz) electrodes and two positivities in the ispilateral anterior basal and parietal electrodes (F9 and P3). The corresponding intracerebral source was localized in the superior bank of the left superior temporal gyrus.

Consistency Validation of Amplitude Maps

Averaged ISS distributions consistency was evaluated using topographic consistency test. When an FDR criterion of 5 % was applied to control for multiple testing, the

Table 2 Anatomical distribution of IIS for each spike network

Patients	IIS networks	Types	Numbers of IIS	Temporal pole			Amy–MTG			Ant. Hipp–ant. MTG			Post. Hipp–post. MTG			Parahipp.–basal T			Mid. hipp–basal T			Insula–STG		
				int	mid	lat	int	mid	lat	int	mid	lat	int	mid	lat	int	mid	lat	int	mid	lat	int	mid	lat
P1	1	M	272				×			**o**									×					
P1	2	M	149				×			×						**o**								
P2	3	M	440				×			×			×			**o**								
P3	4	M	171				×			**o**						×			×					
P3	5	M	94				×			×			**o**						×					
P4	6	M	159				×			×						**o**			×					
P5	7	M	368				×			×			×						**o**					
P6	8	M	248							**o**														
P7	9	M	48				×			**o**						×								
P2	10	M + NC	117	×				×		×			×			**o**								
P3	11	M + NC	166	×	×	×	×			×						×	**o**							
P5	12	M + NC	84	×		×			×	×	×					×	×		**o**	×				
P6	13	M + NC	213		×					**o**				×										
P7	14	M + NC	48	×						×							**o**	×						
P1	15	NC	130						×			×						**o**						
P4	16	NC	668		×						**o**						×			×				
P5	17	NC	64			×			**o**		×									×				
P6	18	NC	122		**o**																			
P6	19	NC	202		**o**				×								×				×			
P7	20	NC	112		×												**o**							
P7	21	NC	173																				**o**	

"×" indicates the presence of epileptic spikes with SNR ≥2 and *bold circles* indicate for the spikes serving as triggers for averaging. *Amy* amygdala, *Hipp* hippocampus, *ITG* inferior temporal gyrus, *MTG* middle temporal gyrus, *STG* superior temporal gyrus, *Parahipp* para-hippocampal, *M* mesial, *NC* neocortical, *M + NC* mesial plus neocortical, *int* internal, *mid* middle, *lat* lateral, *T* temporal, Basal temporal corresponded to fusiform gyrus or inferior temporal gyrus

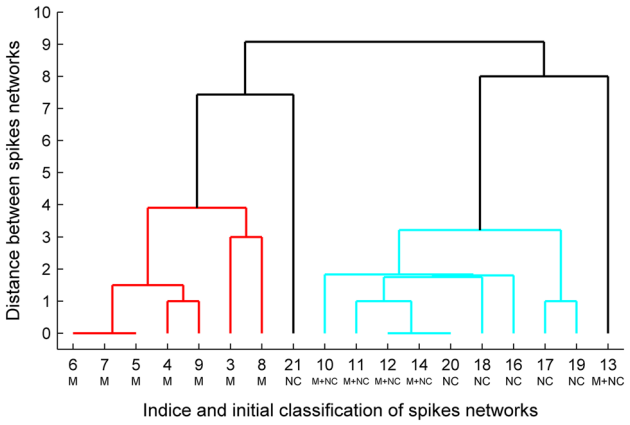

Fig. 5 Topographic consistency test (TCT), applied time-instant by time-instant to the EEG recordings, for the three different spike networks in patient 5. In the upper graphs, the dark line shows the global field power (GFP) computed for all EEG signals ($n = 14$) and for all observations ($n = 368, 84, 64$), the *grey lines* show the GFP of randomly shuffled EEG signals obtained with 500 randomization runs. In the lower graphs, the *dark line* shows the obtained p value, the *dotted line* shows the threshold of a false discovery rate (FDR) of 5 %. Around t_0, the GFP of real data is increasing and the p value is under the threshold indicating the presence of a consistent topography (Color figure online)

threshold of p varied between 0.010 and 0.044 (Table 4). At t_0, topographic consistency tests were always successful and global field powers always higher than these of randomly ($n = 500$) shuffled EEG signals (Fig. 5).

Statistical Analysis of Averaged EEG and Validation of ISS

Most importantly, scalp spikes were recorded in every M network, with a significant negativity in the anterior basal temporal electrode (F9-FT9) that was, however, not specific to M networks (Table 3; Figs. 3, 4). Spikes with a significant negativity in the anterior and basal temporal electrodes were recorded in 20 networks: 90 % in F9–FT9, 82 % in AF7, 80 % in T7 and 67 % in F7. These rates did not significantly differ between the M, M + NC and NC networks. In contrast, a significant concomitant positivity was recorded in the vertex region (Fz, Pz, F3, F4, P4, P3) only in the M + NC and NC networks (Figs. 3, 4). The electrical field of this positivity involved the electrodes F4, C4 or P4 in 50–61 % of cases, Fz, Cz and/or Pz in 38–48 % of cases and C3 or P3 in 38–44 % of cases. Only a single NC network (n21) was discordant with this 3D amplitude map as described in the previous paragraph (Table 3).

Averaged ISS Characteristics

Overall, ISS had an average amplitude of 15 μV in absolute value, a duration of 81 ms and a SNR of 18.0 dB (Table 4). ISS generated by M networks had an average amplitude of 7.1 μV, a duration of 78 ms, and a SNR of 16.1 dB. In contrast, ISS generated by M + NC networks had an average amplitude of 36.1 μV, a duration of 78 ms, and a SNR of 22 dB. Finally, ISS generated by NC networks had an average amplitude of 10 μV, a duration of 87 ms and a SNR of 17.7 dB.

Mean SNR of un-averaged EEG signals varied from −4.9 to 14.4 dB (mean 2.0 dB). ISS generated by M networks had a mean SNR of −2.1 dB, M + NC networks of 8.7 dB and NC networks of 2.4 dB (Table 4). For a network, a negative value of mean SNR indicates that un-averaged amplitudes at t_0 did not differ from the background activity.

Averaged ISS Clusters: Automatic Classification of Amplitude Maps

Two main clusters were obtained from the automatic classification and analysis of the resulting dendrogram (Table 3; Fig. 6). The first cluster included all seven averaged ISS of the M networks and the second cluster included 9 of 11 averaged ISS of the M + NC and NC networks. Two outliers were observed: M + NC network 13 that was characterized by a more widespread positivity involving ipsilateral fronto-central electrodes, and network 21 that was characterized by a fronto-central midline negativity.

Discussion

In this study, we aimed to address the issues of (1) the contribution in scalp EEG of epileptic sources confined to mesial temporal structures, and (2) the distinction of their scalp EEG correlates from those of mesial plus neocortical and neocortical networks.

IIS Networks in Temporal Lobe Epilepsy Comprise Spatially Distributed Sources

In our study, based on SEEG recordings, we first characterized the intracerebral interictal networks that contributed to concomitant scalp EEG signals. A previous study with a similar objective primarily relied on intracranial (foramen ovale) as opposed to intracerebral recordings, without additional subdural electrodes, to characterize medial temporal lobe sources (Merlet et al. 1998). Foramen ovale electrodes, however, placed between the brainstem and the medial temporal lobe, capture the electrophysiological activity generated by both medial and basal temporal generators, thus precluding a differentiation of their respective contribution (Wieser et al. 1985; Eisenschenk

Table 3 Data matrix used for hierarchical clustering and threshold of p for topographic consistency test

Patients	IIS network	Types	Ipsilateral electrodes					Midline electrodes			Contralateral electrodes			FDR criterion: threshold of p
			F9–FT9	AF7–F7 –FP1	F3–F5	C3	P3	Fz	Cz	Pz	P4	C4	F4	
P2	3	M	**−1**	**−1**	**−1**	**−1**	**−1**	***0***	***0***	***0***	***0***	***0***	***0***	0.030
P3	4	M	**−1**	**−1**	***0***	***0***	***0***	***0***	***0***	***0***	***0***	***0***	*1*	0.020
P3	5	M	**−1**	**−1**	***0***	***0***	***0***	***0***	***0***	***0***	***0***	***0***	***0***	0.016
P4	6	M	**−1**	**−1**	***0***	***0***	***0***	***0***	***0***	***0***	***0***	***0***	***0***	0.034
P5	7	M	**−1**	**−1**	***0***	***0***	***0***	***0***	***0***	***0***	***0***	***0***	***0***	0.010
P6	8	M	**−1**	**−1**	***0***	**−1**	**−1**	***0***	***0***	**−1**	**−1**	***0***	***0***	0.024
P7	9	M	**−1**	**−1**	**−1**	***0***	***0***	***0***	***0***	***0***	***0***	***0***	*1*	0.022
P2	10	M + NC	**−1**	**−1**	***0***	*1*	***0***	*1*	*1*	*1*	*1*	*1*	*1*	0.036
P3	11	M + NC	**−1**	**−1**	***0***	*1*	*1*	*1*	*1*	*1*	*1*	*1*	*1*	0.038
P5	12	M + NC	**−1**	**−1**	**−1**	*1*	*1*	*1*	*1*	*1*	*1*	*1*	*1*	0.036
P6	13	M + NC	**−1**	*1*	*1*	*1*	*1*	***0***	***0***	*1*	*1*	***0***	***0***	0.034
P7	14	M + NC	**−1**	**−1**	**−1**	*1*	*1*	*1*	*1*	*1*	*1*	*1*	*1*	0.028
P4	16	NC	**−1**	**−1**	*1*	*1*	*1*	*1*	*1*	*1*	*1*	*1*	*1*	0.038
P5	17	NC	**−1**	**−1**	**−1**	***0***	***0***	*1*	*1*	*1*	*1*	*1*	*1*	0.036
P6	18	NC	***0***	**−1**	***0***	*1*	*1*	*1*	*1*	*1*	*1*	*1*	*1*	0.010
P6	19	NC	**−1**	**−1**	**−1**	***0***	***0***	***0***	*1*	*1*	*1*	*1*	*1*	0.044
P7	20	NC	**−1**	**−1**	**−1**	*1*	*1*	*1*	*1*	*1*	*1*	*1*	*1*	0.026
P7	21	NC	*1*	***0***	***0***	***0***	*1*	**−1**	**−1**	***0***	***0***	***0***	***0***	0.026

−1 and 1 were indicated respectively the presence at t0 of negativity or positivity of ISS in the averaged EEG signals using Walsh's statistical test. Zero indicated that no spike was statistically detected at t0. Thresholds of p were obtained for topographic consistency test with a FDR of 5 % and with 500 randomization runs. *M* mesial, *M + NC* mesial plus neocortical, *NC* neocortical, *SNR* signal to noise ratio, *IIS* interictal intracerebral network, *FDR* false discovery rate

et al. 2001). Moreover, foramen ovale electrodes may miss the contribution of more lateral temporal generators to the concomitant scalp EEG spike. In contrast, SEEG provides a most appropriate methodology in investigating the spatial distribution of epileptic temporal lobe sources since: (1) SEEG allows for the simultaneous recording of all structures from the lateral to mesial aspect of the temporal lobe, including infolded sulcal cortex, with a good spatial resolution (Kahane et al. 2006); (2) SEEG constitutes the only available methodology permitting to record electrophysiological activity directly within cortical sources, as reflected by a phase reversal between contiguous contacts (Jonas et al. 2012) (Fig. 2); (3) SEEG facilitates the distinction of the different sources constituting a given network, as reflected in the common observation of slightly delayed multiple phase reversals between co-occuring intracerebral spikes. SEEG further allows to identify the leader source, generating the earliest and highest amplitude intracerebral spike, within a given network. Thus, in medial temporal networks, the leader source localized either in the anterior hippocampus, the para-hippocampal gyrus, the middle or the posterior hippocampus. These structures have been previously shown to be involved in medial temporal epileptic networks to a different extent (Spencer and Spencer 1994; Bragin et al. 2000; Bartolomei et al. 2008; Bettus et al. 2008). The appreciation of these properties was crucial to correctly identify the leading structure serving as a trigger for each network and thus avoid attributing an intracerebral spike generated by the co-activation of both mesial and neocortical sources solely to a mesial source. Purity of M networks was demonstrated in this study using statistical test and expert analysis that confirmed that non-mesial contacts were not co-activated at t_0: in average less than 7 % of significant responses in non-mesial contacts with a mean amplitude of 7.4 μV.

IIS networks were categorized into one of three predefined categories: mesial, mesial plus neocortical and neocortical. The clinical and neurophysiological relevance of this epileptic network classification in TLE has been previously established (Maillard et al. 2004; Bartolomei et al. 2008). This is the first simultaneous SEEG and EEG study addressing the issue of mesial temporal lobe source contribution to scalp EEG that derives fom a precise characterization of the underlying M, M + NC and NC networks.

Mesial Sources Significantly Contribute to Scalp EEG

The contribution of mesial temporal sources to scalp EEG has been under debate ever since the advent of EEG and SEEG recordings (Abraham and Ajmone-Marsan 1958),

Table 4 Averaged ISS characteristics

Patients	IIS networks	Types	Electrodes	Amplitude (μV)	SNR of averaged signals (dB)	Duration (ms)	Nb. spikes	Mean SNR of un-averaged signals (dB)
P1	1	M	FT9	−2.2	9.7	96	272	−4.8
P1	2	M	FT9	−4.2	9.1	108	149	−2.9
P2	3	M	T7	−8.6	21.6	78	440	−0.7
P3	4	M	FT9	−17.8	22.8	93	171	0.5
P3	5	M	FT9	−11.0	15.2	93	94	−1.0
P4	6	M	FT9	−3.8	13.1	63	159	−4.9
P5	7	M	F9	−5.5	17.2	39	368	−3.5
P6	8	M	P9	−7.0	19.4	45	248	−2.2
P7	9	M	FT9	−3.7	16.6	87	48	0.8
P2	10	M + NC	FT9	−15.6	8.1	95	117	−0.1
P3	11	M + NC	FT9	−64.2	24.1	84	166	13.5
P5	12	M + NC	F9	−43.2	19.5	82	84	6.4
P6	13	M + NC	FT9	−25.6	30.4	63	213	9.1
P7	14	M + NC	FT9	−31.9	27.7	66	48	14.4
P1	15	NC	AF7	−4.8	13.7	103	130	−0.7
P4	16	NC	FT9	−11.1	14.0	95	668	−0.4
P5	17	NC	AF7	−22.7	21.8	79	64	4.7
P6	18	NC	F7	−3.8	17.4	102	122	0.5
P6	19	NC	F7	−11.9	19.8	105	202	7.4
P7	20	NC	FT9	−14.0	25.6	70	112	7.9
P7	21	NC	FZ	−1.5	11.6	55	173	−2.7
			Mean	−15.0	18.0	81	193	2.0

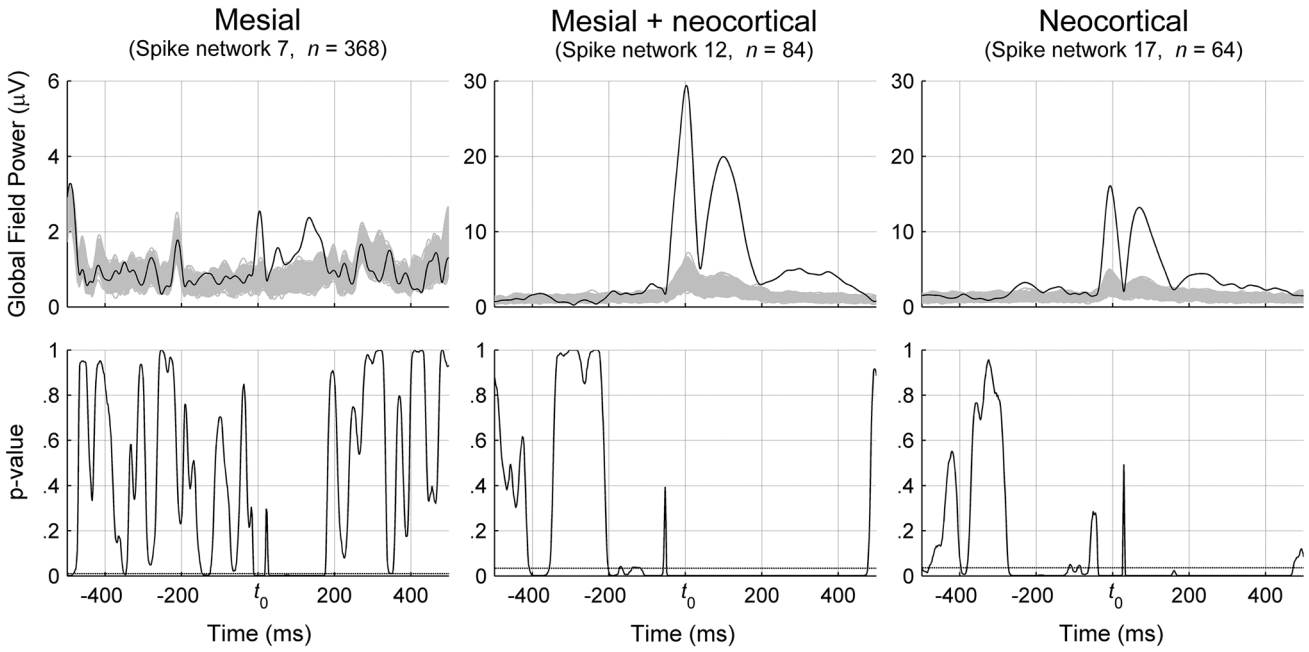

Fig. 6 Hierarchical clustering dendrogram of averaged ISS. All M ISS networks were classified in a same cluster whereas M + NC and NC ISS networks were classified together in another cluster. Two *outliers* were observed in network 13, patient 6, (M + NC network) and in network 21, patient 7 (NC network)

yet remaining unresolved. This might be attributed to: (1) the technical challenge in simultaneously recording SEEG and scalp EEG; (2) the neurophysiological challenge in precisely disentangling the contribution of mesial from neocortical sources to scalp EEG signals.

In our study, we demonstrated that all nine M networks significantly contributed to scalp EEG. The corresponding scalp EEG spikes of M networks always presented a significant negativity recorded in the ispilateral anterior basal temporal electrodes with an average amplitude of 7.1 μV, but no significant positivity. This contribution demonstrates that mesial temporal structures do not generate closed electrical fields despite the folding of the hippocampus and the opposite orientation of the subiculum and parahippocampal gyrus (Jayakar et al. 1991). It further supports that volume conduction also applies to electrical activity generated by deep cortical sources, distant from scalp EEG electrodes.

Regarding closed electrical fields within M networks, it should be noted that epileptic sources were never fully synchronous, as reflected by the 2–10 ms latency between the maximum amplitude of co-occurring mesial temporal spikes. This asynchronous mesial activation may also have contributed to prevent electrical cancellation. This lack of electrical field cancellation in M networks was observed regardless of an additional parahippocampal activation. This parahippocampal co-activation is often overlooked by routine visual interpretation of bipolar SEEG recordings, but has clearly emerged in the condensed amplitude and latency cartographies characterizing the IIS networks. Finally, within M networks, the amplitude of epileptic spikes recorded in the different co-activated structures presented with a great variability (Figs. 2, 3). Therefore, even in cases of synchronous sources localized in geometrically symmetrical structures, such as the opposite banks of a sulcus, the amplitude difference of the resulting electrical fields prevents cancellation.

The average amplitude of ISS generated by M networks, amounting to 7.1 μV, is below the amplitude range of common un-averaged scalp background EEG activity that reportedly ranges from 10 to 50 μV (Chang et al. 2011b). Mean SNR of un-averaged EEG signals of purely M networks (−2.1 dB; max 0.8 dB) also contribute to explain the poor observability of these networks in routine visual interpretation (Gavaret et al. 2004).

Our study is the first in vivo demonstration of sources confined to mesial temporal structures contributing to scalp EEG despite their lack of visibility in routine interpretation. In contrast, spikes generated by M + NC networks had a higher average amplitude of 36.1 μV that is consistent with their superior observability in routine visual interpretation of scalp EEG. The co-activation of mesial and neocortical sources in M + NC networks (e.g. anterior hippocampus, temporal pole, basal temporal area) could render mesial sources detectable in routine visual interpretation. The slightly asynchronous activation of these mesial and neocortical sources facilitates their distinction and delineation by source localization derived from high-resolution EEG (Baumgartner et al. 1995). In our study, we refrained from applying source localization methods on the resulting scalp EEG spikes, due of the limited number of scalp electrodes applied simultaneous to SEEG (Lantz et al. 2003). However, our results suggest that the mesial component of widespread M + NC networks could be accessible to source localization.

MTL Sources Generate Scalp Amplitude Maps Distinct from Those Generated By Neocortical Sources

The negativity of averaged scalp spikes was recorded with the highest amplitude in ipsilateral anterior basal temporal electrodes in 90 % of cases, regardless of the underlying intracerebral temporal network. Therefore, the observation of a scalp EEG negativity in this region cannot be appreciated as a specific marker differentiating mesial from neocortical temporal sources. However, it emphasizes the utility of additional basal-temporal electrodes beyond the commonly applied 10–20 mounting system (Homan et al. 1988) in characterizing interictal networks within the temporal lobe. The more widespread temporal negativity and the midline fronto-parietal positivity of scalp spikes generated by NC and M + NC networks apparently reflected the activation of basal and lateral neocortical areas. At t_0, the topographic consistency test, with a false discovery rate criterion of 5 %, was always successful for every network. Visual inspection of averaged EEG maps was confirmed by this effective method which determines the presence of averaged event-related field using randomization tests (Grouiller et al. 2011).

The hierarchical clustering method allowed to differentiate the scalp electrical fields generated by M networks from those generated by NC and M + NC networks, independent from expert visual evaluation.

The main characteristic of NC and M + NC networks concerned the presence of a significant fronto-centro-parietal positivity. This emphasizes the importance of considering the entire electrical field in a given scalp recording in order to infer the source localization corresponding to an observable spike. This vertex positivity is consistent with the previously reported electrical field in scalp EEG that results from cortical spikes arising from mesial temporal lobe structures as well as adjacent basal and lateral cortical areas (Ebersole and Wade 1991). However, our study further shows that exclusively mesial temporal networks contribute to scalp EEG and generate a distinct electrical field without a significant vertex positivity that clearly differs from networks involving both mesial and basal neocortical areas.

These results can also contribute to the appreciation and delineation of the respective contribution of mesial and basal temporal sources to cognitive scalp potentials evoked by visual categorization and recognition (Maillard et al. 2011). The vertex positivity of M + NC and NC spikes is consistent with the so-called « vertex positive component » of the N170 generated in the ventral temporal areas. On the other hand, the lack of vertex positivity of M spikes renders improbable the contribution of MTL generators to the so-called parietal P600 associated with visual recognition memory (Maillard et al. 2011).

Finally, the demarcation of mesial temporal source contribution to scalp EEG supports the notion that specific biomarkers of these mesial sources could be characterized and detected in the future with signal processing methods without requiring simultaneous invasive recordings and subsequent averaging. These detection methods would rely on the characterization of a mesial interictal scalp spike spatio-temporal template, derived from the current and further simultaneous SEEG and scalp EEG studies.

Conclusion

Mesial temporal sources contribute to scalp EEG despite their deep localization, their curved spatial configuration, and the blurring resulting from the superimposed neocortical activity. Although their contribution is weak, it is detectable by extraction from the respective background activity. Scalp EEG correlates of mesial temporal sources were only detectable in our study with a negativity in the ipsilateral anterior basal temporal electrodes, whereas mesial plus/or neocortical sources were associated with an additional fronto-centro-parietal positivity. This difference was clearly corroborated by the hierarchical clustering method. Our findings prompt further research towards the identification of scalp EEG biomarkers of mesial temporal sources in order to potentially avoid intracerebral recordings in the presurgical evaluation of refractory epilepsy and to serve as a framework for further neurological and cognitive neuroscience applications.

Acknowledgments The Authors would like to thank Cécile Popko (Université de Lorraine) for EEG-SEEG data management. This study was supported by the French Ministry of Health (PHRC 17-05, 2009) and the Regional Council of Lorraine.

References

Abraham K, Ajmone-Marsan CA (1958) Patterns of cortical discharges and their relation to routine scalp electroencephalography. Electroencephalogr Clin Neurophysiol 10:447–461

Alarcon G, Guy CN, Binnie CD, Walker SR, Elwes RD, Polkey CE (1994) Intracerebral propagation of interictal activity in partial activity: implications for source localisation. J Neurol Neurosurg Psychiatry 57:435–449

Alarcon G, Garcia Seoane JJ, Binnie CD, Martin Miguel MC, Juler J, Polkey CE et al (1997) Origin and propagation of interictal discharges in the acute electrocorticogram. Implications for pathophysiology and surgical treatment of temporal lobe epilepsy. Brain 120:2259–2282

Barba C, Barbati G, Minotti L, Hoffmann D, Kahane P (2007) Ictal clinical and scalp-EEG findings differentiating temporal lobe epilepsies from temporal 'plus' epilepsies. Brain 130:1957–1967

Bartolomei F, Wendling F, Bellanger JJ, Régis J, Chauvel P (2001) Neural networks involving the medial temporal structures in temporal lobe epilepsy. Clin Neurophysiol 112:1746–1760

Bartolomei F, Chauvel P, Wendling F (2008) Epileptogenicity of brain structures in human temporal lobe epilepsy: a quantified study from intracerebral EEG. Brain 131:1818–1830

Baumgartner C, Lindinger G, Ebner A, Aull S, Serles W, Olbrich A et al (1995) Propagation of interictal epileptic activity in temporal lobe epilepsy. Neurology 45:118–122

Bettus G, Wendling F, Guye M, Valton L, Régis J, Chauvel P, Bartolomei F (2008) Enhanced EEG functional connectivity in mesial temporal lobe epilepsy. Epilepsy Res 81:58–68

Bragin A, Wilson CL, Engel J Jr (2000) Chronic epileptogenesis requires development of a network of pathologically interconnected neuron clusters: a hypothesis. Epilepsia 41(Suppl 6):S144–S152

Chang BS, Schomer D, Niedermeyer E (2011a) Epilepsy in adults and the elderly. In: Schomer D, Lopes da Silva F (eds) Niedermeyer's electroencephalography: basic principles, clinical applications, and related fields, MD: Wolters-Kluwer Lippincott Williams Wilkins, Baltimore, p 541–562

Chang BS, Schomer D, Niedermeyer E (2011b) Normal EEG and sleep: adults and elderly. In: Schomer D, Lopes da Silva F (eds) Niedermeyer's electroencephalography: basic principles, clinical applications, and related fields. MD: Wolters-Kluwer Lippincott Williams & Wilkins, Baltimore, p 183–214

Chassoux F, Semah F, Bouilleret V, Landre E, Devaux B, Turak B et al (2004) Metabolic changes and electro-clinical patterns in mesio-temporal lobe epilepsy: a correlative study. Brain 127:164–174

Ebersole JS (2000) Sublobar localization of temporal neocortical epileptogenic foci by source modeling. Adv Neurol 84:353–363

Ebersole JS, Wade PB (1991) Spike voltage topography identifies two types of fronto-temporal epileptic foci. Neurology 41:1425–1431

Eisenschenk S, Gilmore RL, Cibula JE, Roper SN (2001) Lateralization of temporal lobe foci: depth versus subdural electrodes. Clin Neurophysiol 112:836–844

Gavaret M, Badier JM, Marquis P, Bartolomei F, Chauvel P (2004) Electric source imaging in temporal lobe epilepsy. J Clin Neurophysiol 21:267–282

Gil-Nagel A, Risinger MW (1997) Ictal semiology in hippocampal versus extra hippocampal temporal lobe epilepsy. Brain 120:183–192

Grouiller F, Thornton RC, Groening K, Spinelli L, Duncan JS, Schaller K et al (2011) With or without spikes: localization of focal epileptic activity by simultaneous electroencephalography and functional magnetic resonance imaging. Brain 134:2867–2886

Harroud A, Bouthillier A, Weil AG, Nguyen DK (2012) Temporal lobe epilepsy surgery failures: a review. Epilepsy Res Treat 2012:201651

Homan RW, Jones MC, Tawat S (1988) Anterior temporal electrodes in complex partial seizures. Electroencephalogr Clin Neurophysiol 70:105–109

Jayakar P, Duchowny M, Resnick TJ, Alvarez LA (1991) Localization of seizure foci: pitfalls and caveats. J Clin Neurophysiol 8:414–431

Jonas J, Descoins M, Koessler L, Colnat-Coulbois S, Sauvée M, Guye M et al (2012) Focal electrical intracerebral stimulation of a

face-sensitive area causes transient prosopagnosia. Neuroscience 222:281–288
Kahane P, Landré E, Minotti L, Francione S, Ryvlin P (2006) The Bancaud and Talairach view on the epileptogenic zone: a working hypothesis. Epileptic Disord 8:S16–S26
Koenig T, Melie-García L (2010) A method to determine the presence of averaged event-related fields using randomization tests. Brain Topogr 23:233–242
Koessler L, Maillard L, Benhadid A, Vignal JP, Felblinger J, Vespignani H et al (2009) Automated cortical projection of EEG sensors: anatomical correlation via the international 10-10 system. Neuroimage 46:64–72
Koessler L, Benar C, Maillard L, Badier JM, Vignal JP, Bartolomei F et al (2010) Source localization of ictal epileptic activity investigated by high resolution EEG and validated by SEEG. Neuroimage 51:642–653
Lantz G, Holub M, Ryding E, Rosén I (1996) Simultaneous intracranial and extracranial recording of interictal epileptiform activity in patients with drug resistant partial epilepsy: patterns of conduction and results from dipole reconstructions. Electroencephalogr Clin Neurophysiol 99:69–78
Lantz G, Grave de Peralta R, Spinelli L, Seeck M, Michel CM (2003) Epileptic source localization with high density EEG: how many electrodes are needed? Clin Neurophysiol 114:63–69
Lieb JP, Walsh GO, Babb TL, Walter RD, Crandall PH (1976) A comparison of EEG seizure patterns recorded with surface and depth electrodes in patients with temporal lobe epilepsy. Epilepsia 17:137–160
Lopes da Silva, Van Rotterdam A (1993) Biophysical aspects of EEG and magnetoencephalogram generation. In: Niedermeyer E, Lopes da Silva F (edn) Electroencephalography: basic principles, clinical applications, and related fields. MD: Williams and Wilkins, Baltimore, p 93–109
Maillard L, Vignal JP, Gavaret M, Guye M, Biraben A, McGonigal A et al (2004) Semiologic and electrophysiologic correlations in temporal lobe seizure subtypes. Epilepsia 45:1590–1599
Maillard L, Koessler L, Colnat-Coulbois S, Vignal JP, Louis-Dorr V, Marie PY (2009) Combined SEEG and source localization study of temporal lobe schizencephaly and polymicrogyria. Clin Neurophysiol 120:1628–1636
Maillard L, Barbeau EJ, Baumann C, Koessler L, Benar C, Chauvel P et al (2011) From perception to recognition memory: time course and lateralization of neural substrates of word and abstract picture processing. J Cogn Neurosci 23:782–800
Merlet I, Gotman J (1999) Reliability of dipole models of epileptic spikes. Clin Neurophysiol 110:1013–1028
Merlet I, Garcia-Larrea L, Ryvlin P, Isnard J, Sindou M, Mauguiere F (1998) Topographical reliability of mesio-temporal sources of interictal spikes in temporal lobe epilepsy. Electroencephalogr Clin Neurophysiol 107:206–212
Mikuni N, Nagamine T, Ikeda A, Terada K, Taki W, Kimura J et al (1997) Simultaneous recording of epileptiform discharges by MEG and subdural electrodes in temporal lobe epilepsy. Neuroimage 5:298–306
Nayak D, Valentín A, Alarcón G, García Seoane JJ, Brunnhuber F, Juler J et al (2004) Characteristics of scalp electrical fields associated with deep medial temporal epileptiform discharges. Clin Neurophysiol 115(6):1423–1435
Ramantani G, Koessler L, Colnat-Coulbois S, Vignal JP, Isnard J, Catenoix H et al (2013) Intracranial evaluation of the epileptogenic zone in regional infrasylvian polymicrogyria. Epilepsia 54:296–304
Sedat J, Duvernoy H (1990) Anatomical study of the temporal lobe. Correlations with nuclear magnetic resonance. J Neuroradiol 17:26–49
Spencer S, Spencer D (1994) Entorhinal-hippocampal interactions in medial temporal lobe epilepsy. Epilepsia 35:721–727
Van 't Ent D, Manshanden I, Ossenblok P, Velis DN, Verbunt JP et al (2003) Spike cluster analysis in neocortical localization related epilepsy yields clinically significant equivalent source localization results in magnetoencephalogram (MEG). Clin Neurophysiol 114(10):1948–1962
Walsh JE (1959) Large sample nonparametric rejection of outlying observations. Ann Inst Stat Math 10:223–232
Wennberg R, Cheyne D (2014) EEG source imaging of anterior temporal lobe spikes: validity and reliability. Clin Neurophysiol 125(5):886–902
Wieser HG (2004) ILAE Commission on Neurosurgery of Epilepsy. ILAE Commission Report. Mesial temporal lobe epilepsy with hippocampal sclerosis. Epilepsia 45:695–714
Wieser HG, Elger CE, Stodieck SR (1985) The 'foramen ovale electrode': a new recording method for the preoperative evaluation of patients suffering from mesio-basal temporal lobe epilepsy. Electroencephalogr Clin Neurophysiol 61:314–322
Williamson PD, Thadani VM, French JA, Darcey TM, Mattson RH, Spencer SS et al (1998) Medial temporal lobe epilepsy: videotape analysis of objective clinical seizure characteristics. Epilepsia 39:1182–1188
Yamazaki M, Tucker DM, Fujimoto A, Yamazoe T, Okanishi T, Yokota T, Enoki H, Yamamoto T (2012) Comparison of dense array EEG with simultaneous intracranial EEG for interictal spike detection and localization. Epilepsy Res 98(2–3):166–173